

# LaVPR: Benchmarking Language and Vision for Place Recognition

Ofer Idan<sup>1</sup> Dan Badur<sup>1</sup> Yosi Keller<sup>1</sup> Yoli Shavit<sup>1</sup>

## Abstract

Visual Place Recognition (VPR) often fails under extreme environmental changes and perceptual aliasing. Furthermore, standard systems cannot perform "blind" localization from verbal descriptions alone, a capability needed for applications such as emergency response. To address these challenges, we introduce LaVPR, a large-scale benchmark that extends existing VPR datasets with over 650,000 rich natural-language descriptions. Using LaVPR, we investigate two paradigms: Multi-Modal Fusion for enhanced robustness and Cross-Modal Retrieval for language-based localization. Our results show that language descriptions yield consistent gains in visually degraded conditions, with the most significant impact on smaller backbones. Notably, adding language allows compact models to rival the performance of much larger vision-only architectures. For cross-modal retrieval, we establish a baseline using Low-Rank Adaptation (LoRA) and Multi-Similarity loss, which substantially outperforms standard contrastive methods across vision-language models. Ultimately, LaVPR enables a new class of localization systems that are both resilient to real-world stochasticity and practical for resource-constrained deployment. Our dataset and code are available at <https://github.com/oferidan1/LaVPR>.

## 1. Introduction

Traditional Visual Place Recognition (VPR) relies on matching global image descriptors to retrieve geo-tagged database entries. However, even state-of-the-art visual models struggle under extreme environmental variations, such as adverse weather, long-term temporal shifts, and motion blur (Lu et al., 2024a). To achieve robust, interactive localization, we propose extending the VPR framework with natural language, focusing on two key paradigms:

<sup>1</sup>Faculty of Engineering, Bar Ilan University, Ramat-Gan, Israel.  
Correspondence to: Yoli Shavit <yoli.shavit@biu.ac.il>.

**Multi-Modal Fusion ( $V + L$ ):** This approach utilizes language as a stable, high-level descriptor to disambiguate visual scenes. By incorporating semantic scene elements and visible text directly into a descriptive narrative, such as "a brick building featuring a 'Pharmacy' sign above the entrance", the system gains a viewpoint-invariant context. While visual degradation can compromise pixel-level features, these linguistic anchors provide a stable reference that maintains retrieval accuracy where vision-only models fail.

**Cross-Modal Retrieval ( $L \rightarrow V$ ):** This paradigm enables "blind" localization, where a system recognizes a place from a textual description alone. This capability is critical for semantic robotics (interpreting human instructions), forensic geolocation (witness descriptions), and emergency rescue calls. For instance, a distressed caller might describe high-stress conditions, e.g., "*someone fainted and I am near a tall stone building with a clock tower*", requiring the system to geolocate the scene solely through linguistic cues. This task requires learning a shared latent space that can align abstract verbal cues with the specific, fine-grained visual features necessary for precise localization.

While these paradigms offer a path toward more resilient localization, mainstream VPR benchmarks are image-only, lacking the textual descriptions required to train and evaluate vision-language models. To address this, we introduce **LaVPR**, a large-scale benchmark comprising over 650,000 descriptions. LaVPR systematically extends established VPR datasets with linguistic data generated via a Visual Large Language Model (VLLM). To ensure spatial fidelity and reduce hallucinations, we employ a segmentation-grounded pipeline and a human-in-the-loop protocol (Section 3).

Using LaVPR, we provide a comprehensive evaluation of vision-language strategies. For Multi-Modal Fusion (Section 4), our results reveal consistent performance gains across a diverse range of visual backbones. Interestingly, we find that linguistic context acts as a universal regularizer: adding language allows compact visual backbones (e.g., ViT-S) to rival the accuracy of larger, compute-intensive models. This offers a path toward high-throughput, efficient deployment. For Cross-Modal Retrieval (Section 5), we observe that standard zero-shot transfer and contrastive fine-tuning fail to achieve precise localization. We instead propose

a parameter-efficient alignment strategy using Low-Rank Adaptation (LoRA) (Hu et al., 2022) in conjunction with a Multi-Similarity (MS) loss (Wang et al., 2019), establishing a robust baseline for cross-modal VPR.

In summary, our contributions are as follows:

- **The LaVPR Benchmark:** We introduce LaVPR, the first standardized, open-source benchmark for vision-language place recognition, extending traditional VPR datasets with over 650,000 aligned textual descriptions.
- **Robust Multi-Modal Fusion:** We demonstrate that language descriptions provide consistent accuracy gains across diverse architectures and datasets, particularly under severe domain shifts. Our analysis reveals that linguistic context acts as a high-level semantic prior, allowing compact backbones to rival the performance of large state-of-the-art vision-only models.
- **LoRA-MS Alignment:** A novel strategy for cross-modal place recognition that integrates Low-Rank Adaptation with Multi-Similarity loss, providing a more discriminative shared latent space that outperforms standard contrastive baselines.

## 2. Related Work

### 2.1. Visual Place Recognition

VPR systems are defined by three primary design choices: the architectural backbone, the aggregation strategy, and the training objective. Backbones have transitioned from standard CNNs (Arandjelovic et al., 2016; Radenović et al., 2018) to Transformer-based models that leverage self-attention for superior global context (Lu et al., 2024a). To compress these features into a global descriptor, methods utilize aggregation strategies such as NetVLAD’s residual clustering (Arandjelovic et al., 2016) or Generalized Mean (GeM) pooling (Radenović et al., 2018). Recent gains involve enhancing these descriptors through attention mechanisms (Huang et al., 2024), multi-scale aggregation (Hausler et al., 2021; Ali-Bey et al., 2023), and adapter-based fine-tuning of foundation models (Lu et al., 2024b). This shift reflects a trend where pre-trained, large-scale encoders provide robust features that often outperform specialized, task-specific architectures. Training typically utilizes contrastive objectives, such as triplet (Hoffer & Ailon, 2015) or multi-similarity loss (Wang et al., 2019), to enforce invariance to environmental changes while maximizing spatial separation. To allow training on dense city-scale datasets, recent methods adopt classification formulations (Bertón et al., 2022; 2023) utilizing large-margin cosine losses (Wang et al., 2018).

The field relies on retrieval metrics (Recall@ $K$ ) across

benchmarks characterized by viewpoint shifts and extreme temporal variations (Yıldız et al., 2022; Torii et al., 2013; 2015). Large-scale training sets like GSV-Cities (Ali-bey et al., 2022) and SF-XL (Bertón et al., 2022) have become standard for these tasks. LaVPR builds on these foundations by augmenting these widely-used datasets with over 650,000 aligned textual descriptions. Unlike previous works limited to uni-modal evaluation, this extension enables a controlled benchmark of multi-modal and cross-modal strategies using identical visual backbones, isolating the impact of linguistic context.

### 2.2. Language-Vision Place Recognition

The exploitation of complementary sensor inputs, and language in particular, remains underexplored for VPR research (Li et al., 2025b).

**Multi-Modal Place Recognition.** Prior fusion methods have predominantly integrated 3D geometry (depth or LiDAR) with imagery (Hu et al., 2020; Piasco et al., 2021; Li et al., 2025a; Komorowski et al., 2021; Lai et al., 2022; Zhou et al., 2023), consistently improving robustness over vision-only approaches. Within the text domain, methods like TextPlace (Hong et al., 2019) have leveraged scene text through Optical Character Recognition (OCR) as an invariant feature, capitalizing on the distinctiveness of street signs and shop names for location identification.

Most recently, MSSPlace (Melekhin et al., 2025) explored fusing diverse data streams, including multi-camera imagery, LiDAR, and text, into a unified global descriptor. To facilitate this, the authors extended the Oxford Robot-Car (Maddern et al., 2017) and NCLT (Carlevaris-Bianco et al., 2015) datasets using MiniGPT-4 (Zhu et al., 2024). While this work provided valuable evidence for the benefits of multi-modal fusion, its evaluation protocol lacked a controlled ablation, comparing multi-modal, multi-view inputs against single-view baselines trained on disparate datasets. Furthermore, the absence of a released dataset or a detailed curation protocol limits the reproducibility of their findings. Our work addresses these limitations by introducing a rigorous, publicly available framework for standardized language-vision place encoding. By maintaining a strictly controlled experimental setup, we isolate the specific contribution of language, revealing new insights into how semantic descriptions complement visual features to achieve robust VPR.

**Cross-Modal Place Recognition.** Research in this area has primarily focused on cross-modal text-to-point-cloud localization (Xia et al., 2024; Xu et al., 2025; Liu et al., 2025). Introduced by Kolmet et al. (Kolmet et al., 2022), this task aims to regress a 6-DoF pose within a 3D environment using only natural language descriptions. Standard pipelines typically employ a coarse-to-fine approach: map-

ping textual queries and 3D sub-maps into a shared embedding space for retrieval, followed by fine-grained matching of semantic instances. Evaluation relies on datasets like KITTI360Pose (Kolmet et al., 2022), an extension of KITTI360 (Xie et al., 2016) containing template-based descriptions of spatial relations. In the text-to-image domain, Shang et al. (2025) recently proposed a multi-view registration approach to align grouped textual descriptions with visual scenes. However, this method diverges from the standard VPR paradigm by requiring multi-view textual queries and focusing on set-to-set alignment rather than scalable, single-query global descriptor retrieval on established benchmarks. In LaVPR, we directly extend VPR training and evaluation benchmarks with textual descriptions, curate them and then analyze the contribution in a controlled setting.

### 3. The LaVPR Benchmark

We introduce LaVPR, a large-scale benchmark designed to bridge visual localization and natural language. By augmenting established VPR datasets with 651,865 aligned descriptions (Table 1), LaVPR enables the systematic evaluation of multi-modal fusion and cross-modal retrieval while preserving original geographic splits for fair comparison.



Figure 1. Example image from the Amstertime-La benchmark. Aligned description in LaVPR: 'Leftmost red brick building with an upper window and a black wrought iron balcony railing, cream-colored framed storefront with a display window, recessed wooden entrance door, narrow brick wall section with house number '3', grey vertical downspout, middle cream-colored framed shop with a glass door, large storefront window displaying "de Witte TandenWinkel", black lower facade panel, red brick upper floor with a rectangular window, blue square sign, grey electrical box, right-most red brick building with an upper window, yellow scalloped awning labeled "KAAS CHEESE"'.

#### 3.1. LaVPR Generation

We employ Gemini 2.5 Flash (Google, 2025) to generate rich, high-density narratives that prioritize permanent architectural features and spatial relationships over transient

elements like pedestrians

Unlike sparse keyword-based datasets, LaVPR provides dense semantic descriptions (Figure 1) that capture fine-grained textures and scene text. This descriptive depth is summarized in Table 3. To isolate the impact of language when vision is compromised, we further curated specialized subsets targeting visual degradation and discriminative scene text (detailed in Table 2). Sections A.2.1- A.2.2 in our Appendix provide the generation prompt and the specialized dataset generation protocols, including example images.

#### 3.2. LaVPR Curation

To mitigate the phenomenon of hallucinations (Huang et al., 2025), we developed a validation pipeline integrating automated *entity extraction* (Phi-3.5-mini-instruct<sup>1</sup>), *spatial grounding* (SAM3<sup>2</sup>), and *binary VLM verification* (Qwen2-VL-7B-Instruct<sup>3</sup>). This automated stage achieves 91% recall and 22% precision on a validation sample; this high-recall profile ensures potential hallucinations are flagged, albeit with many false positives. We manage these via a *Human-in-the-Loop* (HL) phase, where unverified objects are grouped and manually inspected to distinguish true hallucinations from wrongly flagged objects due to out-of-distribution (OOD) issues and visually degraded elements.

We applied this pipeline to all evaluation splits (Appendix Sec. A.3, Table 14). While 26% of samples required secondary verification, HL analysis of the 20 largest unresolved groups revealed that verified hallucinations accounted for only  $\sim 1\%$  of the inspected images. These hallucinations were subsequently removed. Notably, the 1% of flagged hallucinations typically involved only a single erroneous object within an otherwise rich and accurate description. Additional manual validation of in-scene text confirmed a 93.2% accuracy, with minor errors primarily stemming from occlusions or character recognition challenges. For training sets, we prioritized scale by allowing a higher noise ceiling and did not apply further cleaning. We provide a detailed algorithmic walkthrough and ablations of our curation pipeline in the Appendix (Section A.3).

### 4. Multi-Modal Place Recognition ( $L + V$ )

We investigate the synergy between natural language and vision to address the inherent fragility of image-only descriptors. By integrating linguistic context, we provide a stable, high-level semantic reference that persists across temporal and environmental shifts.

<sup>1</sup><https://huggingface.co/microsoft/Phi-3.5-mini-instruct>, Abdin et al. 2024

<sup>2</sup><https://huggingface.co/facebook/sam3>, Carion et al. 2025

<sup>3</sup><https://huggingface.co/Qwen/Qwen2-VL-7B-Instruct>, Wang et al. 2024

Table 1. Overview of the VPR datasets integrated into LaVPR. The combined dataset consists of 651,865 image-description pairs. Dataset characteristics are curated based on (Lu et al., 2024a).

Dataset	Characteristics	Usage	Image Count	
			Database	Queries
GSV-Cities (Ali-bey et al., 2022)	Urban	Train	529,506	–
Pitts30K-Val (Torii et al., 2013)	Urban, Panorama	Validation	10,000	7,608
Pitts30K-Test (Torii et al., 2013)	Urban, Panorama	Test	10,000	6,816
AmsterTime (Yildiz et al., 2022)	Very long-term	Test	1,231	1,231
MSLS-val (Warburg et al., 2020)	Urban, Suburban	Test	18,871	740
MSLS-challenge (Warburg et al., 2020)	Long-term	Test	38,770	27,092
<b>Total (LaVPR)</b>			<b>608,378</b>	<b>43,487</b>

Table 2. Specialized subsets in LaVPR. These datasets target high linguistic discriminativeness and extreme visual domain gaps to isolate the impact of the language channel.

Dataset	Query Characteristics	Search Database	# Queries
Amstertime-La	scene text	Amstertime	31
MSLS-Blur	scene text, blur	MSLS-val	86
MSLS-Weather	scene text, adverse weather	MSLS-val	86

Table 3. Key linguistic and structural statistics of the LaVPR benchmark. These metrics highlight the descriptive density and lexical diversity across the integrated datasets.

Metric	Training	Validation	Test	Total
Total Image-Text Pairs	529,506	17,608	104,751	<b>651,865</b>
Avg. Word Count per Caption	52.78	50.35	46.43	51.69
Avg. Entity Count (Nouns)	23.66	22.49	21.35	23.25
Total Unique Vocabulary	176,893	16,455	55,110	209,200
Signage/Text-heavy Samples (%)	27.77%	55.66%	30.06%	28.89%

#### 4.1. Late-Fusion Methods

We evaluate four late-fusion architectures utilizing frozen, pretrained visual ( $E_v$ ) and textual ( $E_t$ ) encoders. This design isolates cross-modal dynamics and demonstrates the potential of language as a "robustness anchor" without requiring extensive end-to-end retraining.

Given an image  $I$  and description  $t$ , we obtain embeddings  $z_v = E_v(I) \in \mathbb{R}^{d_v}$  and  $z_t = E_t(t) \in \mathbb{R}^{d_t}$ . We explore the following fusion operations:

- Concatenation (CAT): A baseline where  $z_e = [z_v; z_t] \in \mathbb{R}^{d_v+d_t}$ .
- Projection and Addition (PA): Linear layers project both modalities to a shared dimension  $d_e$ , where  $z_e = \text{Linear}(z_v) + \text{Linear}(z_t)$ .
- Multi-Layer Perceptron (MLP): A shallow MLP processes the concatenated vector, expanding the dimension to  $(d_v + d_t)$  before mapping to a fixed latent space  $d_e$ .
- Adaptive Score Fusion (ADS): Instead of feature

fusion, we propose to adaptively weight modality-specific similarity scores (Fig. 12). An MLP with Softmax predicts weights  $W = [w_v, w_t]$  from concatenated query features. For a query-reference pair  $(i, j)$ , weights are averaged:  $w_{m_{ij}} = (w_{m_i} + w_{m_j})/2$  for  $m \in \{v, t\}$ . The joint similarity is  $S_{ij} = w_{v_{ij}} \cdot S_{v_{ij}} + w_{t_{ij}} \cdot S_{t_{ij}}$ .

All fusion modules, except for CAT, are optimized using the Multi-Similarity (MS) loss (Wang et al., 2019):

$$\mathcal{L}_{MS} = \frac{1}{|B|} \sum_{q \in \mathcal{B}} \left\{ \frac{1}{\alpha} \log \left[ 1 + \sum_{p \in \mathcal{P}_q} e^{-\alpha(S_{qp} - \lambda)} \right] + \frac{1}{\beta} \log \left[ 1 + \sum_{n \in \mathcal{N}_q} e^{\beta(S_{qn} - \lambda)} \right] \right\}, \quad (1)$$

where for each query  $q$  in a batch  $B$ ,  $\mathcal{P}_q$  and  $\mathcal{N}_q$  correspond to the sets of positive and negative samples for  $q$ , respectively.  $S_{qp}$  and  $S_{qn}$  are the cosine similarities of a positive pair  $\{q, p\}$  and a negative pair  $\{q, n\}$ .  $\alpha$  and  $\beta$  and  $\lambda$  are hyper-parameters. In ADS, we use the multi-modal similarity scores as input to the multi-similarity loss.

To refine linguistic features, we introduce a Learned Language Pooling (LLP) module, which applies a self-attention mechanism over the hidden states of  $E_t$  to produce a context-aware textual representation. We provide additional implementation and training details in the Section A.5.

#### 4.2. Results & Discussion

We evaluate these fusion strategies across diverse VPR models, including NetVLAD (Arandjelovic et al., 2016), CosPlace (Bertoni et al., 2022), EigenPlaces (Bertoni et al., 2023), MixVPR (Ali-Bey et al., 2023), SALAD (Izquierdo & Civera, 2024), and CricaVPR (Lu et al., 2024a), using BAAI/bge-large-en-v1.5 (BGE-L) model (Xiao et al., 2023) as the primary text encoder.

**Evaluation of Fusion Mechanisms:** As shown in Table 4, ADS and CAT emerge as the most effective strategies. While

Table 4. Comparison of late-fusion mechanisms using MixVPR and BGE-L as the visual and textual backbones, respectively. Shading indicates the best and runner-up multi-modal configurations per dataset.

Fusion	Amstertime				MSLS-val				Pitts30				
	Mechanism	R@1	R@5	R@10	R@20	R@1	R@5	R@10	R@20	R@1	R@5	R@10	R@20
Visual-only		35.7	53.1	60.4	65.9	83.2	91.9	93.4	94.9	90.6	95.6	96.3	97.1
<i>Standard Late Fusion (Without LLP)</i>													
ADS		36.1	53.4	60.5	66.0	<b>83.4</b>	<b>91.9</b>	93.4	94.7	90.7	<b>95.6</b>	96.3	97.1
CAT		37.0	58.2	<b>65.6</b>	71.6	81.9	91.5	93.0	<b>95.9</b>	89.9	95.3	<b>96.4</b>	<b>97.3</b>
MLP		31.7	52.6	59.8	66.6	83.2	91.5	93.0	94.1	89.8	95.1	96.2	97.1
PA		31.0	50.8	57.3	66.0	83.0	90.1	91.9	93.6	89.7	95.1	96.3	<b>97.3</b>
<i>Late Fusion with Learned Language Pooling (LLP)</i>													
ADS		<b>38.1</b>	<b>58.4</b>	64.7	<b>73.5</b>	83.2	91.6	<b>93.5</b>	95.7	<b>90.8</b>	95.4	<b>96.4</b>	<b>97.3</b>
CAT		30.2	51.0	59.7	68.2	77.4	89.1	91.6	93.4	85.7	93.9	95.8	97.0
MLP		32.6	50.8	58.3	65.8	<b>83.4</b>	90.5	92.8	94.2	89.6	95.1	96.2	97.1
PA		30.2	47.5	54.9	63.2	82.3	90.1	92.3	93.9	89.6	94.8	96.1	97.0

Table 5. Comparison of vision-only VPR methods vs. our Language-Augmented (La-) variants using **CAT Fusion** and BGE-L. Bold indicates the best performance within each backbone pair.

Method	Dim	MSLS-Blur			MSLS-Weather			Amstertime-La			MSLS Challenge			Pitts30		
		(d)	R@1	R@5	R@10	R@1	R@5	R@10	R@1	R@5	R@10	R@1	R@5	R@10	R@1	R@5
NetVLAD	32768	24.4	34.9	39.5	25.6	31.4	38.4	19.4	48.4	51.6	27.9	37.0	41.8	<b>82.6</b>	91.6	94.3
La-NetVLAD	+1024	<b>64.0</b>	<b>75.6</b>	<b>82.6</b>	<b>60.5</b>	<b>76.7</b>	<b>82.6</b>	<b>58.1</b>	<b>80.6</b>	<b>80.6</b>	<b>33.0</b>	<b>46.0</b>	<b>51.2</b>	81.8	<b>92.2</b>	<b>94.5</b>
CosPlace	512	46.5	66.3	72.1	67.4	84.9	87.2	48.4	67.7	74.2	57.4	69.9	73.9	89.0	94.7	96.0
La-CosPlace	+1024	<b>67.4</b>	<b>81.4</b>	<b>87.2</b>	<b>87.2</b>	<b>96.5</b>	<b>96.5</b>	<b>54.8</b>	<b>80.6</b>	<b>87.1</b>	<b>60.7</b>	<b>73.7</b>	<b>77.3</b>	<b>89.3</b>	<b>95.0</b>	<b>96.2</b>
EigenPlaces	2048	51.2	76.7	80.2	75.6	88.4	91.9	41.9	64.5	83.9	62.1	73.9	76.4	90.6	95.4	96.8
La-EigenPlace	+1024	<b>73.3</b>	<b>87.2</b>	<b>88.4</b>	<b>87.2</b>	<b>94.2</b>	<b>95.3</b>	<b>48.4</b>	<b>87.1</b>	<b>90.3</b>	<b>64.2</b>	<b>75.5</b>	<b>79.1</b>	<b>90.8</b>	<b>95.7</b>	96.8
MixVPR	512	62.8	76.7	82.6	70.9	86.0	90.7	41.9	80.6	83.9	59.4	72.3	77.3	<b>90.6</b>	<b>95.6</b>	96.3
La-MixVPR	+1024	<b>83.7</b>	<b>94.2</b>	<b>96.5</b>	<b>83.7</b>	<b>94.2</b>	<b>96.5</b>	<b>58.1</b>	<b>90.3</b>	<b>93.5</b>	<b>61.5</b>	<b>74.9</b>	<b>79.9</b>	89.9	95.3	<b>96.4</b>
MixVPR	4096	70.9	82.6	87.2	77.9	83.7	88.4	54.8	80.6	83.9	63.4	76.0	79.2	<b>91.6</b>	<b>95.6</b>	96.4
La-MixVPR	+1024	<b>86.0</b>	<b>98.8</b>	<b>98.8</b>	<b>89.5</b>	<b>95.3</b>	<b>97.7</b>	<b>58.1</b>	<b>87.1</b>	<b>93.5</b>	<b>64.0</b>	<b>76.3</b>	<b>81.1</b>	90.8	95.2	96.4
SALAD	8448	91.9	98.8	98.8	90.7	96.5	97.7	58.1	90.3	93.5	<b>74.6</b>	<b>88.4</b>	<b>91.0</b>	<b>92.2</b>	<b>96.1</b>	<b>97.4</b>
La-SALAD	+1024	<b>93.0</b>	98.8	<b>100</b>	<b>94.2</b>	<b>98.8</b>	<b>100</b>	<b>61.3</b>	<b>93.5</b>	93.5	73.9	87.7	90.1	91.5	96.1	97.1
CricaVPR	10752	91.9	<b>98.8</b>	98.8	88.4	94.2	97.7	<b>64.5</b>	90.3	93.5	<b>69.8</b>	<b>82.2</b>	85.4	<b>93.2</b>	<b>96.7</b>	<b>97.7</b>
La-CricaVPR	+1024	91.9	97.7	98.8	<b>93.0</b>	<b>98.8</b>	<b>100</b>	58.1	<b>93.5</b>	93.5	67.2	81.7	<b>85.8</b>	91.8	96.3	97.5

Table 6. Comparison of vision-only VPR methods vs. our Language-Augmented (La-) variants using **ADS+LLP Fusion** and BGE-L. Bold indicates the best performance within each backbone pair.

Method	Dim	MSLS-Blur			MSLS-Weather			Amstertime-La			MSLS Challenge			Pitts30		
		(d)	R@1	R@5	R@10	R@1	R@5	R@10	R@1	R@5	R@10	R@1	R@5	R@10	R@1	R@5
MixVPR	4096	70.9	82.6	87.2	77.9	83.7	88.4	54.8	80.6	83.9	63.4	76.0	79.2	91.6	95.6	96.4
La-MixVPR	+1024	<b>81.4</b>	<b>93.0</b>	<b>97.7</b>	<b>86.0</b>	<b>91.9</b>	<b>96.5</b>	<b>61.3</b>	<b>90.3</b>	<b>94.8</b>	<b>76.9</b>	<b>80.3</b>	<b>91.9</b>	<b>95.7</b>	<b>96.7</b>	
SALAD	8448	91.9	98.8	98.8	90.7	96.5	97.7	58.1	90.3	93.5	74.6	88.4	91.0	92.2	96.1	<b>97.4</b>
La-SALAD	+1024	<b>93.0</b>	98.8	98.8	<b>94.2</b>	<b>98.8</b>	<b>100</b>	<b>61.3</b>	90.3	93.5	<b>74.6</b>	<b>88.8</b>	<b>91.2</b>	<b>92.3</b>	<b>96.3</b>	<b>97.4</b>
CricaVPR	10752	91.9	<b>98.8</b>	98.8	88.4	94.2	97.7	64.5	90.3	93.5	69.8	<b>82.2</b>	85.4	93.2	96.7	97.7
La-CricaVPR	+1024	<b>93.0</b>	<b>98.8</b>	<b>98.8</b>	<b>94.2</b>	<b>98.8</b>	<b>98.8</b>	64.5	<b>96.8</b>	<b>96.8</b>	<b>70.2</b>	82.1	<b>86.1</b>	<b>93.3</b>	96.7	97.7

CAT performs well on Pitts30, ADS achieves peak robustness on MSLS-val. Notably, LLP acts as a catalyst for ADS, improving R@1 on Amstertime to 38.1. Conversely, CAT performance degrades when combined with LLP, suggesting that adaptive weighting benefits more from refined semantic pooling than fixed concatenation. Results in Tables 5 and 6 suggest a scaling trend: CAT effectively handles

lower-dimensional descriptors (e.g., MixVPR-512), while ADS+LLP provides greater robustness for larger backbones like CricaVPR.

**Consistent Gains and Compensatory Dynamics:** Tables 5 and 6 show that language-augmented (La-) methods consistently outperform visual-only baselines. We observe that

Table 7. Relative R@1 Gain (%) of Language-Augmented (La-) methods compared to visual-only baselines. **Positive gains** indicate linguistic complementarity; **negative values** indicate slight degradation.

Method	Fusion	Backbone (Dim)	Pretraining	Loss	Relative R@1 Gain (%) per Dataset				
					MSLS-B	MSLS-W	Ams.	MSLS-C	Pitts30
La-NetVLAD	CAT	VGG16 (32k)	SUP (IN-1k)	TRP	+162.3	+136.3	+199.5	+18.3	-1.0
La-CosPlace	CAT	ResNet50 (512)	SUP (IN-1k)	LMC	+44.9	+29.4	+13.2	+5.7	+0.3
La-EigenPlace	CAT	ResNet50 (2k)	SUP (IN-1k)	LMC	+43.2	+15.3	+15.5	+3.4	+0.2
La-MixVPR	CAT	ResNet50 (4k)	SUP (IN-1k)	MS	+21.3	+14.9	+6.0	+0.9	-0.9
La-MixVPR	ADS+LLP	ResNet50 (4k)	SUP (IN-1k)	MS	+14.8	+10.4	+11.9	+2.2	+0.3
La-SALAD	CAT	DinoV2-L (8k)	SSL (DINO)	MS	+1.2	+3.9	+5.5	-0.9	-0.8
La-SALAD	ADS+LLP	DinoV2-L (8k)	SSL (DINO)	MS	+1.2	+3.9	+5.5	0.0	+0.1
La-CricaVPR	CAT	DinoV2-L (10k)	SSL (DINO)	MS	0.0	+5.2	-9.9	-3.7	-1.5
La-CricaVPR	ADS+LLP	DinoV2-L (10k)	SSL (DINO)	MS	+1.2	+6.6	0.0	+0.6	+0.1

Pretraining Abbreviations: SUP (IN-1k): Supervised on ImageNet-1k; SSL (DINO): Self-supervised Invariance-based (DINOv2).

Loss Abbreviations: TRP: Triplet; LMC: Large Margin Cosine; MS: Multi-Similarity.

Table 8. Efficiency-Performance Trade-off: Comparing CricaVPR and La-CricaVPR (ours) with smaller backbones and CAT fusion. Computation details for parameter count and GFLOPS for query encoding (Inference) and Retrieval are provided in Section A.4.

Configuration	Params (M)	Complexity (GFLOPs)			Dim (d)	MSLS-Blur		MSLS-Weather		Amstertime-La	
		Inf.	Retr.	Total		R@1	R@5	R@1	R@5	R@1	R@5
CricaVPR (Base, SOTA)	106.8	17.5	0.20	17.7	10k	91.9	<b>98.8</b>	88.4	94.2	<b>64.5</b>	90.3
CricaVPR-Small	27.2	4.6	0.10	4.8	5k	89.5	95.3	84.9	91.9	54.8	87.1
<b>La-Crica-Small</b>	60.6	6.7	0.12	6.82	6k	<b>93.0</b>	97.7	<b>90.7</b>	<b>96.5</b>	58.1	<b>93.5</b>

\*La-Crica-Small corresponds to CricaVPR with ViT-S + BGE-Small. It achieves higher R@1 than the Base SOTA model with  $\sim 62\%$  fewer Total GFLOPs.

Table 9. Impact of Textual Encoders on Visual Place Recognition.

Fusion	Text Encoder	Dim	MSLS-Blur		MSLS-Weather		Amstertime-La		Pitts30	
			R@1	R@5	R@1	R@5	R@1	R@5	R@1	R@5
<i>Text-only Baselines</i>										
None	BGE-S	384	57.0	80.2	57.0	80.2	25.8	58.1	37.3	60.9
None	BGE-L	1024	54.7	74.4	54.7	74.4	38.7	67.7	36.5	62.4
None	ModernBert-L	1024	60.5	76.7	60.5	76.7	35.5	58.1	37.1	61.8
<i>Multi-modal: Visual Backbone (MixVPR 512)</i>										
Visual Only	-	512	62.8	76.7	70.9	86.0	41.9	80.6	<b>90.6</b>	<b>95.6</b>
CAT	BGE-S	+384	83.7	94.2	88.4	<b>96.5</b>	58.1	87.1	90.1	95.2
	BGE-L	+1024	83.7	94.2	83.7	94.2	58.1	<b>90.3</b>	89.9	95.3
	ModernBert-L	+1024	81.4	91.9	86.0	95.3	<b>61.3</b>	83.9	90.7	95.2
ADS+LLP	BGE-S	+384	87.2	95.3	<b>89.5</b>	<b>96.5</b>	48.4	83.9	90.0	95.1
	BGE-L	+1024	<b>89.5</b>	96.5	88.4	94.2	58.1	<b>90.3</b>	88.8	94.8
	ModernBert-L	+1024	87.2	<b>98.8</b>	88.4	<b>96.5</b>	<b>61.3</b>	<b>90.3</b>	88.6	94.7

linguistic context serves as a critical compensatory signal in adverse conditions; La-methods exhibit double-digit relative gains on subsets characterized by extreme blur and weather. In these scenarios, language functions as a discriminative anchor that remains invariant to the visual domain shifts that otherwise suppress pixel-level features. A qualitative example, comparing MixVPR and La-MixVPR is further illustrated in Fig. 2.

**Influence of Pre-training Paradigms and Backbone Architecture:** The magnitude of performance gains is closely tied to the visual backbone’s pre-training objective and its architecture (Table 7). Supervised convolutional back-



Figure 2. Qualitative results (Amstertime dataset). From left to right: Query, MixVPR Top-1, La-MixVPR Top-1 (using CAT Fusion). Correct matches are bordered in green; incorrect in red. Additional Results are provided in the Appendix, Section A.7.

bones (VGG and ResNet) show the most significant relative improvements, with NetVLAD achieving gains up to 200% R@1. This suggests that supervised classification

pre-training leaves "semantic gaps" regarding environmental context that language effectively bridges. Conversely, Self-Supervised (SSL) Transformer backbones like DINOv2 show smaller relative gains (< 7%), as their invariance-based objectives capture a richer set of visual-semantic relationships. However, the consistent 6.6% gain for CricaVPR on MSLS-Weather demonstrates that even advanced SSL Transformer backbones benefit from the descriptive granularity of language when visual reliability is compromised.

**Computational Efficiency and Scaling:** Language integration offers a path toward efficient deployment (Table 8). By pairing a compact visual backbone (CricaVPR with ViT-Small) with a lightweight text encoder (BGE-Small), we achieve 93.0 R@1 on MSLS-Blur, outperforming the massive visual-only CricaVPR-Base. This hybrid approach reduces computational complexity by 62% (6.82 GFLOPs vs. 17.7 GFLOPs), demonstrating that horizontal scaling via multi-modality is a more efficient route to robustness than the vertical scaling of transformers architectures.

**Effect of Text Encoder:** Table 9 highlights that larger state-of-the-art language encoders (e.g., ModernBERT-Large (Warner et al., 2025)) excel in semantically dense environments like Amstertime-La (61.3% R@1). However, in degraded visual conditions (Blur/Weather), performance is uniform across encoder sizes (e.g., BGE-S and BGE-L). This implies that while complex scenes require sophisticated linguistic discrimination, simple "semantic anchoring" is sufficient to overcome visual noise.

**Complementary Synergy versus Sequential Retrieval:** Finally, we compare our joint approach against sequential re-ranking (Top-100 retrieval followed by cross-modal re-ranking). As shown in Table 10, sequential ranking fails catastrophically (R@1 drops to 1.2%) due to the retrieval bottleneck: if the primary modality misses the ground truth in the initial top- $K$ , the second cannot recover it. Furthermore, candidates that rank highly in one modality do not necessarily possess discriminative features in the other. Joint fusion avoids this by allowing both modalities to mutually disambiguate the search space from the start.

*Table 10.* Comparison of Joint Fusion (Ours) vs. Sequential Re-ranking on Amstertime. Sequential methods re-rank the top-100 candidates from the initial search modality.

Initial Search	Re-ranked by	Amstertime (Recall@K)			
		R@1	R@5	R@10	R@20
<i>Single Modality Baselines</i>					
MixVPR (Visual)	-	35.7	53.1	60.4	65.9
BGE (Textual)	-	9.5	18.0	23.5	32.4
<i>Sequential Re-ranking (Top-100)</i>					
MixVPR	BGE (Text)	1.2	3.4	5.2	6.6
BGE	MixVPR (Vis)	4.4	5.6	5.9	6.3
<i>Joint Multi-modal Fusion</i>					
LaVPR (Ours)	-	<b>37.0</b>	<b>58.2</b>	<b>65.6</b>	<b>71.6</b>

## 5. Cross-Modal Place Recognition ( $L \rightarrow V$ )

While multi-modal fusion leverages language as a robust auxiliary signal, a more fundamental challenge lies in Cross-Modal Retrieval ( $L \rightarrow V$ ): identifying a geographic location within a visual database using only a natural language query. This task necessitates a strict alignment between abstract linguistic descriptions and the concrete, structural visual features that define a specific place.

### 5.1. Aligning Language and Vision for 'Blind' Localization

Given an image  $I$  and a textual description  $t$ , let  $E_v$  and  $E_t$  denote the visual and textual encoders mapping  $I$  and  $t$  to embeddings  $\mathbf{z}_v \in \mathbb{R}^{d_v}$  and  $\mathbf{z}_t \in \mathbb{R}^{d_t}$ , respectively. The objective is to retrieve the ground-truth image  $I^*$  from a database  $\mathcal{D}$  that corresponds to a query description  $t_q$ . To bridge the gap between these disparate latent spaces, we employ Low-Rank Adaptation (LoRA) (Hu et al., 2022). For a pre-trained weight matrix  $W_0 \in \mathbb{R}^{d \times k}$ , the weight update is represented as a low-rank decomposition:

$$W = W_0 + \Delta W = W_0 + BA \quad (2)$$

where  $B \in \mathbb{R}^{d \times r}$  and  $A \in \mathbb{R}^{r \times k}$ , with rank  $r \ll \min(d, k)$ . We apply these updates to all linear projections within the Transformer layers of our vision-language backbones. The model is optimized using the Multi-Similarity (MS) loss (Eq. 1), which encourages a discriminative cross-modal manifold by mining hard positive and negative pairs across modalities. We provide additional training and implementation details and qualitative examples in Sections A.6-A.7.

### 5.2. Results & Discussion

**The Challenge of Zero-Shot Alignment:** Results in Table 11 show that standard vision-language foundation models (CLIP (Radford et al., 2021), BLIP (Li et al., 2022), EvaClipv2 (Fang et al., 2024), SigLIPv2 (Tschanne et al., 2025)) exhibit poor zero-shot performance, with R@1 scores frequently below 3%. This underscores a fundamental "semantic-structural gap": generic semantic representations optimized for object-level concepts lack the fine-grained architectural cues essential for localization. Our experiments show that both isolated Learned Pooling and full fine-tuning with MS loss lead to catastrophic failure ( $R@1 \approx 0.1\%$ ), likely because the visual-discriminative objectives of VPR conflict with the broad semantic priors of frozen text encoders.

**Consistent Efficacy of PEFT and MS Alignment:** We observe a consistent and substantial performance gain across all evaluated architectures when utilizing Parameter-Efficient Fine-Tuning (PEFT) via LoRA. As detailed in Table 11, our La-variants provide an order-of-magnitude improvement over their respective baseline models. For

Table 11. Cross-modal Vision-Language Retrieval performance. We compare cross-modal foundation models against our language-augmented (**La-**) versions. Bold indicates the best result within each model pair.

Model	Amstertime				MSLS-val				Pitts30			
	R@1	R@5	R@10	R@20	R@1	R@5	R@10	R@20	R@1	R@5	R@10	R@20
CLIP	2.0	7.5	12.1	18.0	2.3	6.2	10.4	14.5	10.9	29.6	43.5	59.6
La-CLIP	<b>11.5</b>	<b>27.5</b>	<b>37.7</b>	<b>50.4</b>	<b>38.0</b>	<b>58.4</b>	<b>68.2</b>	<b>77.2</b>	<b>49.3</b>	<b>74.4</b>	<b>82.8</b>	<b>89.7</b>
BLIP	1.3	4.1	7.0	12.3	1.6	5.9	8.2	11.6	8.1	26.8	41.1	56.7
La-BLIP	<b>12.8</b>	<b>31.4</b>	<b>41.1</b>	<b>53.2</b>	<b>38.0</b>	<b>60.5</b>	<b>68.4</b>	<b>75.4</b>	<b>50.2</b>	<b>74.2</b>	<b>82.8</b>	<b>89.6</b>
EVA-CLIP-V2	2.8	8.0	12.7	18.1	3.8	9.2	13.0	19.1	11.4	30.9	44.2	59.9
La-EVA-V2	<b>11.5</b>	<b>27.9</b>	<b>36.8</b>	<b>47.8</b>	<b>32.8</b>	<b>52.8</b>	<b>62.4</b>	<b>70.9</b>	<b>41.5</b>	<b>66.8</b>	<b>76.6</b>	<b>85.1</b>
SigLIP-V2	0.9	3.1	5.5	8.8	2.6	6.5	9.7	13.1	10.1	30.1	44.3	61.9
La-SigLIP-V2	<b>13.8</b>	<b>29.0</b>	<b>40.0</b>	<b>49.5</b>	<b>35.7</b>	<b>60.5</b>	<b>69.6</b>	<b>76.2</b>	<b>49.3</b>	<b>74.6</b>	<b>82.8</b>	<b>89.2</b>

Table 12. Comparison of training strategies for Cross-modal VPR.

Training Strategy	Loss	Amstertime (Recall@K)			
		R@1	R@5	R@10	R@20
Zero-shot	Frozen Encoders	1.3	4.1	7.0	12.3
LLP	MS	0.1	0.5	1.0	2.4
Full Fine-tuning	MS	0.1	0.4	0.9	1.6
LoRA (All Linear, $r = 64$ )	Contrastive	0.1	0.4	0.8	1.6
LoRA (All Linear, $r = 64$ )	<b>MS</b>	<b>12.8</b>	<b>31.4</b>	<b>41.1</b>	<b>53.2</b>

Table 13. Ablation of LoRA hyperparameters and Loss functions for Cross-modal VPR.

Target Layers	Rank ( $r$ )	Loss	Amstertime (Recall@K)			
			R@1	R@5	R@10	R@20
LoRA (QKV)	16	Contrastive	4.0	10.1	13.9	19.9
LoRA (QKV)	16	MS	8.9	25.0	34.0	44.8
LoRA (QKV)	64	MS	10.6	29.1	38.0	49.3
LoRA (All Linear)	64	Contrastive	0.1	0.4	0.8	1.6
LoRA (All Linear)	<b>64</b>	<b>MS</b>	<b>12.8</b>	<b>31.4</b>	<b>41.1</b>	<b>53.2</b>

instance, La-SigLIP-V2 reaches an R@1 of 13.8 on Amstertime and 35.7 on MSLS-val, compared to 0.9 and 2.6 for the base model. Notably, on the Pitts-30k benchmark, La-SigLIP-V2 R@5 performance peaks at 74.6%, rising from a baseline of 30.0%. This trend remains stable across different backbones, confirming that LoRA successfully injects domain-specific VPR knowledge while preventing the catastrophic forgetting. We further carry out ablations using the BLIP model.

**Ablation of Training Strategy:** Our training strategy ablation (Table 12, rows 2–5) reveals that the combination of LoRA and the Multi-Similarity (MS) loss is the primary driver of convergence. We find that standard adaptation techniques are insufficient; both isolated LLP and full fine-tuning with MS loss result in near-total failure ( $R@1 \approx 0.1\%$ ). Furthermore, using LoRA with a standard contrastive objective (the original BLIP loss) yields markedly lower performance. It is only the synergy be-

tween the parameter-efficient capacity of LoRA and the hard-mining capabilities of the MS loss, explicitly designed for the retrieval-heavy VPR task, that enables the model to bridge the semantic-structural gap.

**LoRA Configuration and Coverage:** Our ablations in Table 13 indicate that the scope of adaptation is as critical as the rank itself. Targeting all linear layers outperforms targeting only  $Q$ ,  $K$ ,  $V$  matrices. Extending coverage across all projections with rank  $r = 64$  provides the necessary capacity to capture complex environmental semantics, yielding a peak R@1 of 12.8% on Amstertime. This suggests that the structural nuances required for VPR are distributed throughout the Transformer blocks, necessitating a comprehensive adaptation of both attention and feed-forward mechanisms.

## 6. Conclusion

**Limitations and Future Work.** In this work, we focused on late-fusion that may overlook geometric inter-dependencies accessible via early- or mid-fusion. We also observe diminishing returns for state-of-the-art self-supervised backbones, where linguistic context can introduce sub-optimal priors when visual features are already highly discriminative. Furthermore, a substantial performance gap persists between cross-modal and uni-modal retrieval despite LoRA-MS gains. Future work will investigate more sophisticated alignment objectives, additional modalities and token-level interactions.

**Summary.** This work introduces LaVPR, a large-scale benchmark that extends vision-only datasets with high-density linguistic descriptions to investigate multi-modal and cross-modal localization. Our analysis demonstrates that language serves as a critical robustness anchor; specifically, our ADS-LLP mechanism yields consistent gains and superior computational efficiency compared to the vertical scaling of visual transformers. Finally, we establish that the synergy between LoRA and Multi-Similarity (MS) loss is essential for effective cross-modal retrieval, providing order-of-magnitude improvements over standard baselines.

## References

Abdin, M. I., Ade Jacobs, S., Awan, A. A., et al. Phi-3 technical report: A highly capable language model locally on your phone. Technical Report MSR-TR-2024-12, Microsoft, August 2024. URL <https://arxiv.org/abs/2404.14219>.

Ali-bey, A., Chaib-draa, B., and Giguere, P. Gsv-cities: Toward appropriate supervised visual place recognition. *Neurocomputing*, 2022.

Ali-Bey, A., Chaib-Draa, B., and Giguere, P. Mixvpr: Feature mixing for visual place recognition. In *Proceedings of the IEEE/CVF winter conference on applications of computer vision*, pp. 2998–3007, 2023.

Arandjelovic, R., Gronat, P., Torii, A., Pajdla, T., and Sivic, J. Netvlad: Cnn architecture for weakly supervised place recognition. In *Proceedings of the IEEE conference on computer vision and pattern recognition*, pp. 5297–5307, 2016.

Bertoni, G., Masone, C., and Caputo, B. Rethinking visual geo-localization for large-scale applications. In *Proceedings of the IEEE/CVF Conference on Computer Vision and Pattern Recognition*, pp. 4878–4888, 2022.

Bertoni, G., Trivigno, G., Caputo, B., and Masone, C. Eigen-places: Training viewpoint robust models for visual place recognition. In *Proceedings of the IEEE/CVF International Conference on Computer Vision*, pp. 11080–11090, 2023.

Carion, N., Gustafson, L., Hu, Y.-T., Debnath, S., Hu, R., Suris, D., Ryali, C., Alwala, K. V., Khedr, H., Huang, A., et al. Sam 3: Segment anything with concepts. *arXiv preprint arXiv:2511.16719*, 2025.

Carlevaris-Bianco, N., Ushani, A. K., and Eustice, R. M. University of Michigan North Campus long-term vision and lidar dataset. *International Journal of Robotics Research*, 35(9):1023–1035, 2015.

Caron, M., Touvron, H., Misra, I., Jégou, H., Mairal, J., Bojanowski, P., and Joulin, A. Emerging properties in self-supervised vision transformers. In *Proceedings of the IEEE/CVF international conference on computer vision*, pp. 9650–9660, 2021.

Fang, Y., Sun, Q., Wang, X., Huang, T., Wang, X., and Cao, Y. Eva-02: A visual representation for neon genesis. *Image and Vision Computing*, pp. 105171, 2024.

Google. Gemini 2.5 flash, 2025. URL <https://deepmind.google/technologies/gemini/>.

Hausler, S., Garg, S., Xu, M., Milford, M., and Fischer, T. Patch-netvlad: Multi-scale fusion of locally-global descriptors for place recognition. In *Proceedings of the IEEE/CVF conference on computer vision and pattern recognition*, pp. 14141–14152, 2021.

Hoffer, E. and Ailon, N. Deep metric learning using triplet network. In *International workshop on similarity-based pattern recognition*, pp. 84–92. Springer, 2015.

Hong, Z., Petillot, Y., Lane, D., Miao, Y., and Wang, S. Textplace: Visual place recognition and topological localization through reading scene texts. In *Proceedings of the IEEE/CVF International Conference on Computer Vision*, pp. 2861–2870, 2019.

Hu, E. J., Shen, Y., Wallis, P., Allen-Zhu, Z., Li, Y., Wang, S., Wang, L., Chen, W., et al. Lora: Low-rank adaptation of large language models. *ICLR*, 1(2):3, 2022.

Hu, H., Qiao, Z., Cheng, M., Liu, Z., and Wang, H. Dasgil: Domain adaptation for semantic and geometric-aware image-based localization. *IEEE Transactions on Image Processing*, 30:1342–1353, 2020.

Huang, G., Zhou, Y., Hu, X., Zhang, C., Zhao, L., and Gan, W. Dino-mix enhancing visual place recognition with foundational vision model and feature mixing. *Scientific Reports*, 14(1):22100, 2024.

Huang, L., Yu, W., Ma, W., Zhong, W., Feng, Z., Wang, H., Chen, Q., Peng, W., Feng, X., Qin, B., et al. A survey on hallucination in large language models: Principles, taxonomy, challenges, and open questions. *ACM Transactions on Information Systems*, 43(2):1–55, 2025.

Izquierdo, S. and Civera, J. Optimal transport aggregation for visual place recognition. In *Proceedings of the ieee/cvf conference on computer vision and pattern recognition*, pp. 17658–17668, 2024.

Kaplan, J., McCandlish, S., Henighan, T., Brown, T. B., Chess, B., Child, R., Gray, S., Radford, A., Wu, J., and Amodei, D. Scaling laws for neural language models. *arXiv preprint arXiv:2001.08361*, 2020.

Kolmet, M., Zhou, Q., Ošep, A., and Leal-Taixé, L. Text2pos: Text-to-point-cloud cross-modal localization. In *Proceedings of the IEEE/CVF Conference on Computer Vision and Pattern Recognition*, pp. 6687–6696, 2022.

Komorowski, J., Wysoczańska, M., and Trzcinski, T. Min-kloc++: lidar and monocular image fusion for place recognition. In *2021 International Joint Conference on Neural Networks (IJCNN)*, pp. 1–8. IEEE, 2021.

Lai, H., Yin, P., and Scherer, S. Adafusion: Visual-lidar fusion with adaptive weights for place recognition. *IEEE Robotics and Automation Letters*, 7(4):12038–12045, 2022.

Li, J., Li, D., Xiong, C., and Hoi, S. Blip: Bootstrapping language-image pre-training for unified vision-language understanding and generation. In *International conference on machine learning*, pp. 12888–12900. PMLR, 2022.

Li, K., Ou, Y., Ning, J., Kong, F., Cai, H., and Li, H. Unified depth-guided feature fusion and reranking for hierarchical place recognition. *Sensors*, 25(13):4056, 2025a.

Li, Z., Shang, T., Xu, P., and Deng, Z. Place recognition meet multiple modalities: a comprehensive review, current challenges and future development. *Artificial Intelligence Review*, 58(11):363, 2025b.

Liu, D., Huang, S., Li, W., Shen, S., and Wang, C. Text to point cloud localization with multi-level negative contrastive learning. In *Proceedings of the AAAI Conference on Artificial Intelligence*, volume 39, pp. 5397–5405, 2025.

Lu, F., Lan, X., Zhang, L., Jiang, D., Wang, Y., and Yuan, C. Cricavpr: Cross-image correlation-aware representation learning for visual place recognition. In *Proceedings of the IEEE/CVF Conference on Computer Vision and Pattern Recognition*, pp. 16772–16782, 2024a.

Lu, F., Zhang, L., Lan, X., Dong, S., Wang, Y., and Yuan, C. Towards seamless adaptation of pre-trained models for visual place recognition. In *The Twelfth International Conference on Learning Representations*, 2024b. URL <https://openreview.net/forum?id=TVg6h1fsKa>.

Maddern, W., Pascoe, G., Linegar, C., and Newman, P. 1 year, 1000 km: The oxford robotcar dataset. *The International Journal of Robotics Research*, 36(1):3–15, 2017.

Melekhin, A., Yudin, D., Petryashin, I., and Bezuglyj, V. Mssplace: Multi-sensor place recognition with visual and text semantics. *IEEE Access*, 2025.

Oquab, M., Dariseti, T., Moutakanni, T., Vo, H., Szafraniec, M., Khalidov, V., Fernandez, P., Haziza, D., Massa, F., El-Nouby, A., et al. Dinov2: Learning robust visual features without supervision. *arXiv preprint arXiv:2304.07193*, 2023.

Piasco, N., Sidibé, D., Gouet-Brunet, V., and Demonceaux, C. Improving image description with auxiliary modality for visual localization in challenging conditions. *International Journal of Computer Vision*, 129(1):185–202, 2021.

Radenović, F., Tolias, G., and Chum, O. Fine-tuning cnn image retrieval with no human annotation. *IEEE transactions on pattern analysis and machine intelligence*, 41(7):1655–1668, 2018.

Radford, A., Kim, J. W., Hallacy, C., Ramesh, A., Goh, G., Agarwal, S., Sastry, G., Askell, A., Mishkin, P., Clark, J., et al. Learning transferable visual models from natural language supervision. In *International conference on machine learning*, pp. 8748–8763. PMLR, 2021.

Shang, T., Li, Z., Xu, P., Qiao, J., Chen, G., Ruan, Z., and Hu, W. Bridging text and vision: A multi-view text-vision registration approach for cross-modal place recognition. *arXiv preprint arXiv:2502.14195*, 2025.

Torii, A., Sivic, J., Pajdla, T., and Okutomi, M. Visual place recognition with repetitive structures. In *Proceedings of the IEEE conference on computer vision and pattern recognition*, pp. 883–890, 2013.

Torii, A., Arandjelovic, R., Sivic, J., Okutomi, M., and Pajdla, T. 24/7 place recognition by view synthesis. In *Proceedings of the IEEE conference on computer vision and pattern recognition*, pp. 1808–1817, 2015.

Tschannen, M., Gritsenko, A., Wang, X., Naeem, M. F., Alabdulmohsin, I., Parthasarathy, N., Evans, T., Beyer, L., Xia, Y., Mustafa, B., et al. Siglip 2: Multilingual vision-language encoders with improved semantic understanding. *Localization, and Dense Features*, 6, 2025.

Wang, H., Wang, Y., Zhou, Z., Ji, X., Gong, D., Zhou, J., Li, Z., and Liu, W. Cosface: Large margin cosine loss for deep face recognition. In *Proceedings of the IEEE conference on computer vision and pattern recognition*, pp. 5265–5274, 2018.

Wang, P., Bai, S., Tan, S., Wang, S., Fan, Z., Bai, J., Chen, K., Liu, X., Wang, J., Ge, W., et al. Qwen2-vl: Enhancing vision-language model’s perception of the world at any resolution. *arXiv preprint arXiv:2409.12191*, 2024.

Wang, X., Han, X., Huang, W., Dong, D., and Scott, M. R. Multi-similarity loss with general pair weighting for deep metric learning. In *Proceedings of the IEEE/CVF conference on computer vision and pattern recognition*, pp. 5022–5030, 2019.

Warburg, F., Hauberg, S., Lopez-Antequera, M., Gargallo, P., Kuang, Y., and Civera, J. Mapillary street-level sequences: A dataset for lifelong place recognition. In *Proceedings of the IEEE/CVF conference on computer vision and pattern recognition*, pp. 2626–2635, 2020.

Warner, B., Chaffin, A., Clavié, B., Weller, O., Hallström, O., Taghadouini, S., Gallagher, A., Biswas, R., Ladhak, F., Aarsen, T., et al. Smarter, better, faster, longer: A

modern bidirectional encoder for fast, memory efficient, and long context finetuning and inference. In *Proceedings of the 63rd Annual Meeting of the Association for Computational Linguistics (Volume 1: Long Papers)*, pp. 2526–2547, 2025.

Xia, Y., Shi, L., Ding, Z., Henriques, J. F., and Cremers, D. Text2loc: 3d point cloud localization from natural language. In *Proceedings of the IEEE/CVF conference on computer vision and pattern recognition*, pp. 14958–14967, 2024.

Xiao, S., Liu, Z., Zhang, P., Wang, N., , et al. C-pack: Packged resources for general chinese embedding. *arXiv preprint arXiv:2309.07597*, 2023.

Xie, J., Kiefel, M., Sun, M.-T., and Geiger, A. Semantic instance annotation of street scenes by 3d to 2d label transfer. In *Proceedings of the IEEE conference on Computer Vision and Pattern Recognition*, pp. 3688–3697, 2016.

Xu, Y., Qu, H., Liu, J., Zhang, W., and Yang, X. Cmmloc: Advancing text-to-pointcloud localization with cauchy-mixture-model based framework. In *Proceedings of the Computer Vision and Pattern Recognition Conference*, pp. 6637–6647, 2025.

Yildiz, B., Khademi, S., Siebes, R. M., and Van Gemert, J. Amstertime: A visual place recognition benchmark dataset for severe domain shift. In *2022 26th International Conference on Pattern Recognition (ICPR)*, pp. 2749–2755. IEEE, 2022.

Zhou, Z., Xu, J., Xiong, G., and Ma, J. Lcpr: A multi-scale attention-based lidar-camera fusion network for place recognition. *IEEE Robotics and Automation Letters*, 9 (2):1342–1349, 2023.

Zhu, D., Chen, J., Shen, X., Li, X., and Elhoseiny, M. MiniGPT-4: Enhancing vision-language understanding with advanced large language models. In *The Twelfth International Conference on Learning Representations*, 2024. URL <https://openreview.net/forum?id=1tZbq88f27>.

## A. Appendix

The following sections provide a deep dive into the experimental and algorithmic foundations of our work:

- **LaVPR Generation & Specialized Subsets:** We provide the standardized prompts used for large-scale description generation and detail the curation protocols for specialized challenge sets, including signage-based filtering for Amstertime-La and synthetic augmentations for MSLS-Blur/Weather.
- **Curation Pipeline Walkthrough:** A detailed algorithmic description of our four-step curation process is provided, covering automated object extraction, open-set detection, and VLM-based verification designed to mitigate hallucinations. We provide analysis of our curation process and ablations for our cleaning strategy.
- **Efficiency & Complexity Analysis:** We provide the details for the GFLOP and parameter count derivations used to evaluate the trade-offs between architectural scaling and retrieval performance.
- **Implementation Details:** Specific training configurations, hardware specifications, and hyperparameter settings are listed for both multi-modal fusion (including ADS and CAT) and cross-modal retrieval (LoRA and MS-loss) paradigms.
- **Qualitative Results:** We present a collection of representative samples from the LaVPR dataset alongside visual comparisons between baseline MixVPR and our proposed La-MixVPR, illustrating success cases in challenging urban environments.

### A.1. LaVPR Generation: Extended Details

### A.2. Qualitative Examples

We provide selected samples from the LaVPR dataset in Figures 3-6.



*Figure 3.* Example image from the Amstertime subset. *Generated description in LaVPR:* Light-colored brick building with multiple windows, blue ground-level door with a round window, dark gray ornate pillar, teal/turquoise framed glass door with "ORION" logo, teal/turquoise shopfront with display windows behind a metal security gate, green and purple "NIRVANA T-SHIRT GALLERY" sign, red and white striped awning, teal/turquoise ornate double door, dark gray ornate pillar with number "3" and graffiti, black facade with vertical red and black diamond pattern, white door with number "54" above it, brick sidewalk..



*Figure 4.* Example image from the Amstertime subset. *Generated description in LaVPR:* A multi-story reddish-brown brick building facade with numerous white-framed windows and light-colored stone accents; from left to right: a partial large arched window with white grilles, a section of brick with a vertical stack of two rectangular white-framed windows, a large rectangular sign integrated into the brick facade reading "DE SAVORNIN LOHMAN SCHOOL." with orange lettering and light-colored borders, a section of brick with two upper small arched windows and two lower rectangular white-framed windows, a central large arched brick entrance containing double dark wooden doors, above which are three small arched windows, a rectangular light-colored plaque on the brick wall inscribed with "CHRISTELIJKE SCHOOL M.U.L.O. TEGELAAR", a section of brick with a vertical stack of two rectangular white-framed windows, and a partial large arched window with white grilles.



*Figure 5.* Example image from the MSLS-Val subset. *Generated description in LaVPR:* Green trees, blue overhead road sign pointing left to "Hillerød 16" and "Frederikssund 211", asphalt road with white lane markings, red traffic lights at an intersection, blue overhead road sign pointing straight to "O2 16", blue overhead road sign pointing straight to "Centrum", asphalt road with "BUS" painted on it and a white left-turn arrow marking a bicycle lane, rows of red-brick buildings with white-framed windows, large red-brick building with numerous white-framed windows, a sidewalk.



*Figure 6.* Example image from the MSLS-Val subset. *Generated description in LaVPR:* Large multi-story red brick corner building with dark windows, shops on ground floor; pedestrian crossing markings on asphalt road; double white lines on road separating lanes; white left-turn arrow painted on road; traffic light pole; sequence of buildings further down the street including modern light-colored building with horizontal windows; blue circular street sign; multi-story red brick building on right; light yellow-beige shop facade with "FASAN BAGERIET" sign and golden pretzel symbols; "BUS" lane marking painted on road.

#### A.2.1. PRIMARY GENERATION PROMPT

To ensure consistent, high-density descriptions across 651,865 image-text pairs, we utilized Gemini 2.5 Flash with the following standardized prompt:

"Describe this location for visual place recognition. Focus on: 1) Scene type and setting, 2) Distinctive landmarks and architecture, 3) Unique visual patterns/colors/textures, 4) Spatial layout, 5) Key identifying features that distinguish this place from similar locations. Be specific about permanent visual elements, avoid temporary objects like people, cars, weather and lighting conditions, provide textual descriptions of items you are certain about only. the output is one line of text listing the items from left to right, separated by commas."

We experimented with similar prompts and found the VLLM to yield relatively stable descriptions.

#### A.2.2. SPECIALIZED DATASET GENERATION PROTOCOLS

To evaluate the limits of language-vision complementarity, we curated specialized subsets targeting specific VPR challenges: semantic distinctiveness (Amstertime-La) and visual degradation (MSLS-Blur/Weather). These subsets facilitate a controlled analysis of how linguistic context compensates for pixel-level information loss.

**Signage-based Filtering (Amstertime-La):** This subset targets locations with high discriminative potential. We utilized Gemini 2.5 Flash to identify and filter database-query pairs where specific signage text matched exactly across both images. Qualitative examples of these high-precision alignments are shown in Figure 7.

We used the following prompt for filtering:

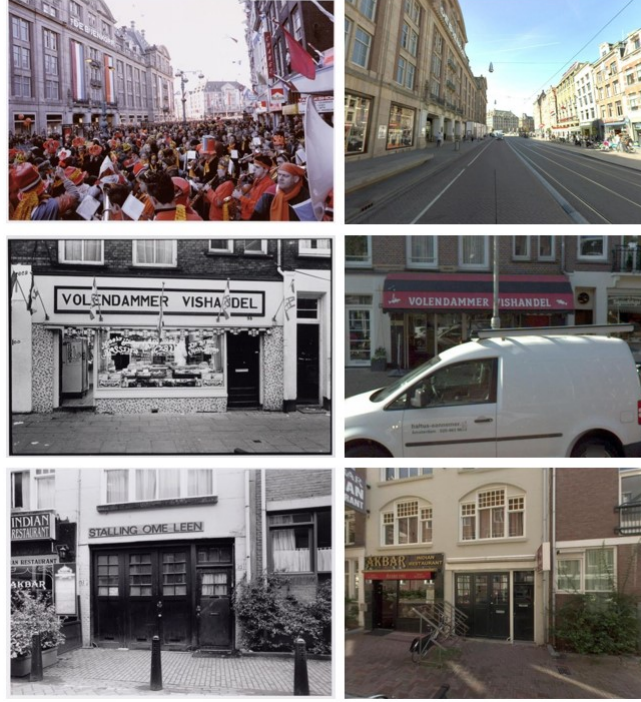


Figure 7. Example pairs from the Amstertime-La dataset. The dataset is curated by identifying shared signage and scene text between query (left) and database (right) images to ensure fine-grained semantic alignment.

”filter images of same place where the sign text is the same between database and query.

for example:

queries/image1.jpg, ”INDIAN RESTAURANT AKBAR signage, framed menu display, street number 151, planter with green foliage, dark bollard, brick-patterned pavement, STALLING OME LEEN sign, large dark double doors with glass panes, smaller dark single door with glass panes and mail slot, street number 19, dark bollard, brick-patterned pavement, brick wall with dense green ivy, ground-floor window with white curtains.”

database/image1.jpg, ”Leftmost building fragment with partial sign, light-colored building with two upper arched multi-paned windows, AKBAR INDIAN RESTAURANT sign, red awning, restaurant entrance door, dark double-door entrance, metal bike rack, brown brick building with upper window and black balcony railing, lower white-framed window, green shrubbery, reddish-brown brick pavement.”

both have sign with text of AKBAR INDIAN RESTAURANT. put the result in table format.”

**Visual Degradation Synthesis (MSLS Subsets):** To further simulate extreme operational environments, we applied synthetic transformations to the MSLS-val queries. For BLUR augmentations, we used Photoshop’s Lens Blur tool. We further utilized gemini-nano-banana to generate adverse weather conditions (e.g., heavy rain, snow, and fog) with the following prompt:

”Transform this image. Make it look like snow, with strong rain and a lot of fog. Add icicles to the buildings and trees.”

The visual characteristics of these augmentations are illustrated in Figure 8.

### A.3. LaVPR Curation: Extended Details

#### A.3.1. CURATION PIPELINE: ALGORITHMIC WALKTHROUGH

Enriching standard VPR training and evaluation datasets with aligned natural language descriptions, using a state-of-the-art Vision–Language Model, requires a strategy that accounts for model reliability constraints. Although Gemini Flash 2.5 is



Figure 8. Example images from MSLS-Blur and MSLS-Weather subset, left is original query image, middle is blurred augmentation, right is augmented with rain, snow and fog.

widely regarded as a state-of-the-art model, we lacked a concrete quantitative assessment of its performance, beyond general expectations reported in the literature (Google, 2025).

Given the natural variability in human image descriptions, we prioritized descriptive accuracy over completeness. Consequently, we designed and developed a pipeline to validate the presence of objects and scene elements mentioned in the generated descriptions.

Given an image–description pair  $(I, D)$ , our pipeline applies the following four steps:

1. **Object Extraction.** Given the generated description  $D$ , we use a large language model (LLM) to extract a list of mentioned objects  $\mathcal{O}_D$ .
2. **Open-Set Object Detection.** We provide the image  $I$  together with  $\mathcal{O}_D$  as input to an open-set object detector, to localize all mentioned objects in the image. Figure 9 provides an example output of this step.
3. **VLM-Based Verification.** For each object that is not detected in the previous step, we perform an additional verification step using a vision–language model. Specifically, we ask a binary (yes/no) question to determine whether the object can be visually identified in the image.
4. **Textual Object Filtering.** From the remaining objects that are still not found in the image, we use an LLM to automatically filter out objects categories that correspond to textual elements, contain special characters, or objects that are deemed undetectable (for example: "sunlight").

After applying this procedure to all image–description pairs, we aggregate the remaining objects across pairs, group them by unique object notion, and rank the groups by frequency. Next, we manually inspect the top object groups (we set  $K = 20$  for the test and validation datasets) and assign each group to one of the following categories (qualitative illustrations presented in Figure 11):

- **Hallucination:** Objects that do not appear in the image and are considered hallucinated by the Vision–Language model we used to generate the text descriptions.
- **Visually Degraded:** Objects that are extremely small, heavily occluded, or located at the image boundaries.
- **Out-of-Distribution (OOD):** Long-tail or rare objects that fall outside the models’ distribution used in steps 2 and 3 of our pipeline.

For each group, the labeling decision is made by visually inspecting a small sample of object instances from that group. Finally, to mitigate hallucinations, we edit the generated descriptions by removing only the objects belonging to the

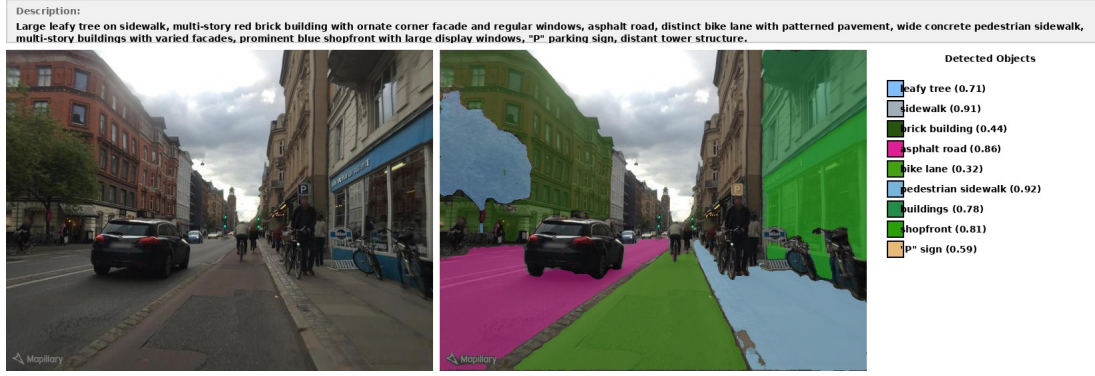


Figure 9. Qualitative visualization of Step 2: Open-set object detection using SAM3. Given an input image and a set of object queries extracted from the generated description, SAM3 produces segmentation masks for visually identifiable objects.

Table 14. Unified Pipeline Statistics: Models and Filtering Progression. "Remaining" columns indicate the % of descriptions that passed all checks up to that step. The remaining descriptions were grouped by category and HL was applied to the top-20 categories.

Pipeline Stage	Model / Framework	Primary Function	Descriptions Remaining after Step (%)				
			Ams.	MSLS-val	MSLS-challenge	Pitts-T	Pitts-V
1. Entity Extraction	Phi-3.5-mini-instruct	Entity extraction from text	100%	100%	100%	100%	100%
2. Grounding	SAM3	Spatial localization (confidence thresh. = 0.2)	68%	66%	66%	67%	65%
3. Verification	Qwen2-VL-7B-Instruct	Binary hallucination check	39%	36%	35%	33%	32%
4. Object Filtering	Phi-3.5-mini-instruct	Selective token removal	29%	28%	26%	23%	23%

Hallucination category from their generated descriptions they were extracted from. Figure 10 further illustrates the entire pipeline schema.

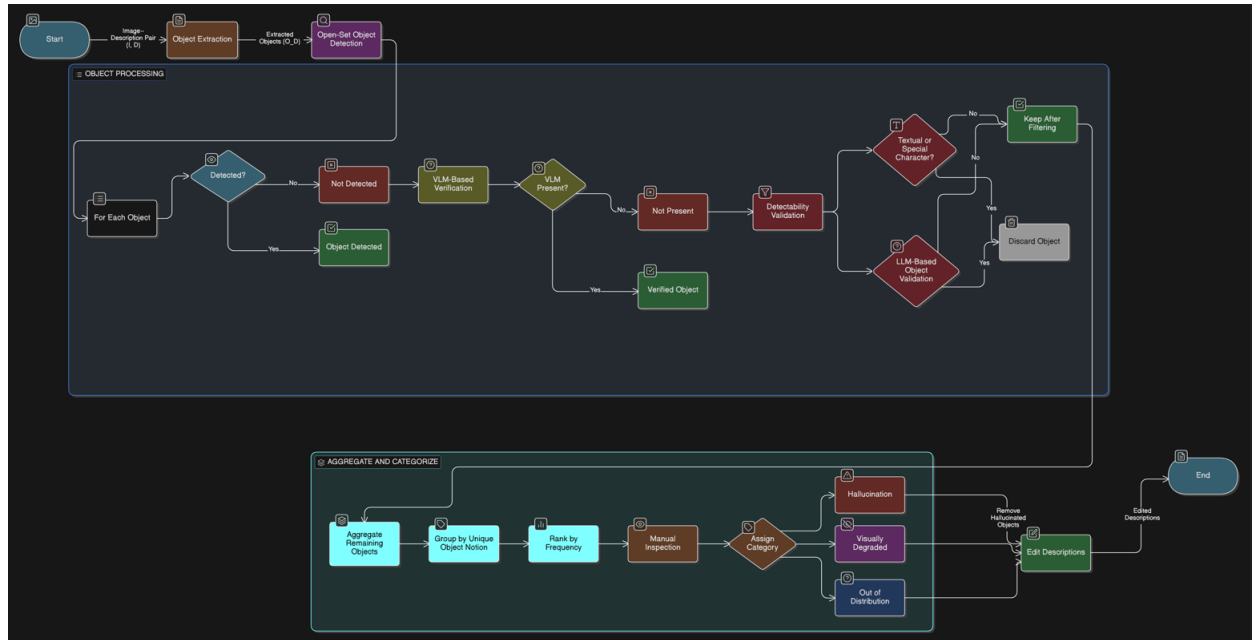


Figure 10. LaVPR Curation Pipeline Diagram

### A.3.2. CURATION ANALYSIS

We ran our pipeline on the validation and test datasets listed in Table 1. Across all datasets, approximately 26% of the combined database and query samples remained after Step 4 (see Table 14). After aggregation, we obtained 6,336 unique object groups. Manual inspection of the 20 largest groups showed that 15 corresponded to out-of-distribution (OOD) objects, while the remaining 5 contained visually degraded content. Overall, descriptions flagged as containing hallucinations and subsequently sent for cleaning accounted for  $\sim 1\%$  of the inspected images within the top-20 categories.



Figure 11. Examples of unresolved object categories. **Left:** Hallucinated object (low dark metal railing). **Middle:** Visually degraded object (buildings heavily obscured). **Right:** Out-of-distribution object (embankment).

### A.3.3. MANUAL VALIDATION OF IN-SCENE SIGNAGE

We perform further human-in-the-loop verification on Amstertime-La and MSLS-Val to ensure the accuracy of in-scene signage. This step specifically addresses textual elements that elude automated segmentation, providing a high-precision ground truth for discriminative scene text. We manually analyzed 117 images and their corresponding texts. The analysis demonstrated that descriptions are predominantly accurate with rich detail that supports fine-grained location discrimination, as illustrated in Figure 1. Nevertheless, minor inaccuracies were observed, primarily in signage labels that were occluded or due to occasional character recognition errors, still most of the signage labels were correct, reaching an accuracy of 93.2% on our samples images.

### A.3.4. CLEANING STRATEGY ABLATION

We evaluate several dataset refinement strategies to identify the optimal balance between descriptive density and semantic accuracy (Table 15). Under the 'Full Clean' strategy, an LLM is utilized to purge all objects identified by our pipeline as candidate hallucinations. Conversely, the 'Hybrid' strategy, detailed in Section A.3.1, employs manual verification of high-frequency flagged categories to selectively determine which entities to remove. For both methodologies, we utilize Llama-3.3-70B-Instruct for automated entity removal. We also compare these strategies to a permissive strategy, which applies description curation. The marginal performance variance observed across these strategies suggests that noise level is initially relatively low (consistent with our curation analysis). Results also indicate a slight advantage to permissive strategies, suggesting that models can handle local sparse hallucinations (one hallucinated object within a rich and dense description).

Table 15. Effect of cleaning strategies on retrieval performance. Results are reported for La-MixVPR using CAT fusion and BGE-L as the text encoder.

Cleaning Strategy	Amstertime (Recall@K)			
	R@1	R@5	R@10	R@20
None (Baseline)	<b>37.0</b>	<b>58.2</b>	<b>65.6</b>	<b>71.6</b>
Hybrid	<b>37.0</b>	<b>58.2</b>	65.5	<b>71.6</b>
Full	36.6	58.0	65.0	<b>71.6</b>

### A.3.5. PIPELINE IMPLEMENTATION: PROMPTS AND MODELS

- *Step 1 (caption  $\rightarrow$  objects + stuff extraction, Phi-3.5-mini-instruct):*

I want to use both an object detector and a segmentation model to check the correctness of an image caption obtained by an image caption model. Can you help to parse the caption below and list: (1) All objects that could be detected with an object detection model in the image, and (2) All uncountable regions (stuff) that could be segmented in the image. Examples of stuff: road, grass, pavement, wall, sidewalk, water, ground. Stuff are materials, surfaces, or regions rather than individual objects. Please ignore sky. Please ignore dynamic objects like people and cars. Please only list the object/region names and ignore descriptions like colors. Please use singular for all listed items. Please do not list signs or surfaces with written words. Here are some examples of the desired behavior in the format of caption and expected output:

Example 1

Caption: Green utility box/door set in a brick wall, dense green foliage and trees along the left side, paved sidewalk, asphalt road with double yellow lines and white ""DISABLED"" marking, paved sidewalk, black ornate street lamp post, dark metal railings, row of brown brick terraced houses with white window frames and white ground floor sections, distant buildings.

utility box. brick wall. green foliage. tree. sidewalk. asphalt road. street lamp post. railings. terraced houses. white window frames. buildings. ### END\_OF\_LIST ###

Example 2

Caption: White painted brick wall (upper left), dark brick facade with white-framed multi-pane sash window (upper left), dark brick facade with black-framed door and black iron balcony (upper center), dark brick facade with white-framed multi-pane sash window (upper right), dark grey tiled sloped roof (lower center), black framed door/window unit (lower left), large white-framed multi-pane sash window (lower center), white wall with black wall-mounted lantern and silver intercom/doorbell panel (lower right), black garage door with a narrow window above it (lower right), vertical cream/yellow pipe (far right).

wall. window. door. balcony. roof. pipe ### END\_OF\_LIST ###

Example 3

Caption: River Thames with distant buildings and boats, ornate dark lamppost with criss-cross patterns, bridge parapet with dark top rail and decorative light-on-red criss-cross panels, blue road sign with bus and bicycle pictograms, light-colored lamppost on a column base, grey paved walkway, ""BUS"" road marking with a red line.

River. lamppost. bridge parapet. road. sign. walkway ### END\_OF\_LIST ###

Now do the same for this new caption. Caption: caption. Please concatenate all objects and stuff together with "." as separation. Do not add any explanation, notes, headings, or markdown; output only the concatenated object and region names. After the last item, output exactly ### END\_OF\_LIST ### and nothing else.

- **Step 3 (vision-language yes/no checker, *Qwen2-VL-7B-Instruct*):**

Answer strictly with 'yes' or 'no'. Is there a 'obj' clearly visible in this image?

Example:

Input: Answer strictly with 'yes' or 'no'.

Is there a 'tree canopies' clearly visible in this image?  
 Expected output: yes.

#### A.4. Efficiency-Performance Trade-off Analysis

Table 8 presents a comparative analysis between the baseline CricaVPR variants and our proposed Language-Augmented (LA) Small variant utilizing CAT fusion. For this evaluation, we adopt the model parameter counts for CricaVPR as reported in (Lu et al., 2024a). For CricaVPR-Small which uses DinoV2-Small as its backbone (Oquab et al., 2023; Caron et al., 2021), similar to CricaVPR, we added the adapters to its parameters count. BGE-Small parameter count is based on (Xiao et al., 2023), where we used the model's english version.

#### General GFLOPS Calculation for Transformers

Following the methodology of Kaplan et al. (2020), the computational cost  $C$  for a Transformer forward pass over a sequence of length  $S$  is approximated by:

$$C \approx 2NS \text{ FLOPs} \quad (3)$$

where  $N$  denotes the number of non-embedding parameters,  $S$  represents the sequence length in tokens, and the factor of 2 accounts for multiply-accumulate (MAC) operations, comprising one multiplication and one addition per token.

The CricaVPR-Small architecture employs a hidden dimension of 384 with 6 attention heads, whereas the CricaVPR-Base variant incorporates 768 dimensions and 12 attention heads. This architectural scaling yields a  $4\times$  increase in floating-point operations (FLOPs), thereby providing enhanced representational capacity at the expense of substantially higher computational overhead. CricaVPR's input image resolution is 224x224.

For the BGE-Small model, the computational cost is estimated as  $C \approx 2NS \approx 2.1$  GFLOPs, where  $N \approx 21.2\text{M}$  denotes the non-embedding parameters and  $S = 50$  represents the sequence length (average caption length as seen in Table 3).

We evaluate the total computational complexity by partitioning the pipeline into two primary stages:

1. **Inference:** The forward pass through the CricaVPR backbone to extract the image embedding vector.
2. **Retrieval:** The vector search phase, which calculates similarity metrics (e.g., cosine similarity) between the query embedding and the database entries.

The total parameter count for our *LA-Crica-Small* model is calculated as the summation of the parameters from the CricaVPR-Small and BGE-Small architectures.

#### A.5. Multi-Modal VPR: Implementation Details

We trained several late fusion architectures using frozen VPR backbones and a frozen text encoder backbone (BGE). The fusion architectures evaluated include CAT, PA, MLP, and ADS. All techniques were trained on the same dataset, adhering to the standard GSV-Cities framework augmented with our textual descriptions, which provides a highly accurate dataset comprising 67k places represented by 529k images. We employed the Multi-Similarity loss function for training, using  $\alpha=1$ ,  $\beta=50$  and margin=0. Each training batch contained  $P = 120$  places, with 4 images per place, yielding mini-batches of 480 images. Optimization was performed using Stochastic Gradient Descent (SGD) with a momentum of 0.9 and weight decay of 0.001. The initial learning rate was set to 0.05 and reduced by a factor of 3 every 2 epochs. Training proceeded for a maximum of 10 epochs on an NVIDIA RTX 3090 GPU equipped with 24GB VRAM.

Figure 12 depicts the ADS+LLP fusion approach. The LLP employs an attention mechanism in which each token is processed through a linear layer, after which a softmax function calculates the importance score  $Si$  for each token. The embedding of each token (excluding the CLS token) is then weighted by its corresponding  $Si$  value to generate a pooled representation. This pooled token is concatenated with the CLS token and subsequently passed through an additional linear layer followed by a Tanh activation function, yielding the final embedding.

#### A.6. Cross-Modal VPR: Implementation Details

We trained multiple architectures (learned pooling, LoRA, full fine-tuning) with different loss functions (Contrastive and Multi-Similarity loss) across various VLM encoders, using  $\alpha=2$ ,  $\beta=40$  and margin=0.5. In all cases, training was applied to

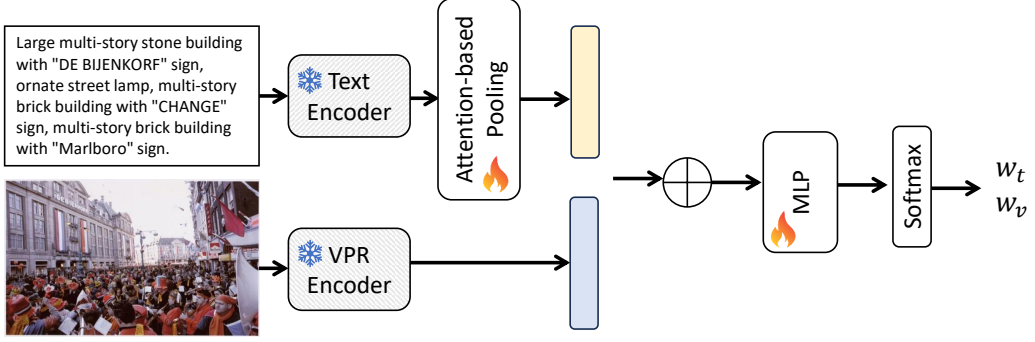


Figure 12. Illustration of the ADS+LLP Fusion Method.

both the visual and textual encoders. Training batches consisted of  $P = 60$  places, each represented by 4 images, resulting in mini-batches of 240 images. We employed Stochastic Gradient Descent (SGD) with momentum 0.9 and weight decay of 0.001. The initial learning rate of 0.05 was divided by 3 every 2 epochs, and training was conducted for a maximum of 10 epochs. Experiments were performed on an NVIDIA H200 GPU with 141GB VRAM. For all models used for evaluation (Blip, SigLip etc.) we have used the Base version.

We further investigated an approach involving two separate pooling layers trained on top of a frozen image encoder (MixVPR, DinoV2) and a frozen text encoder (BGE). We observed that the training process did not converge and yielded poor performance.

#### A.7. Qualitative Results for Multi-Modal and Cross-Modal Place Recognition

Figures 13-15 show selected examples of retrieval results using MixVPR and La-MixVPR (ours) for multi-modal place recognition. Figures 16-18 compare cross-modal place recognition with BLIP and La-BLIP.



Figure 13. Qualitative comparison between MixVPR (top) and La-MixVPR (bottom) on the Amstertime dataset. La-MixVPR uses BGE-Large as the text encoder with CAT fusion. From left to right: Query, Top-1, Top-2, and Top-3 retrieved images. Green borders indicate a correct match, while red borders indicate an incorrect match.



(a) MixVPR



Vertical building edge with mosaic-like tiles, vertical house number "100" on the tiled edge, open doorway entrance, poster depicting a cat inside the left doorway, large shop display window, multiple irregularly shaped white signs with dark text and numbers (including "2.80") placed inside the shop window, shop sign with "VOLENDAMMER VISHANDEL" in dark capital letters on a white background, several small flags with horizontal stripes and a symbol hanging above the shop window, street number "98" below the "VISHANDEL" sign, closed dark door with a letter slot, building column/wall to the right of the closed door covered with mosaic-like tiles, white vertical downspout, red brick facade of the building on the upper floor, white-framed rectangular windows on the upper floor, paved sidewalk in the foreground.



Light-colored building with multi-paned glass ground floor door/window, brick upper facade with white-framed windows, red and black horizontally striped retractable awning displaying "VOLENDAMMER VISHANDEL" in white capital letters flanked by white fish silhouettes, large glass storefront windows, dark vertical pole, adjacent light-colored facade with dark-framed opening, brick upper facade with white balcony with black railings, storefront with "kapadokya" sign in white script.



Ornate dark brown wooden facade building with two large ground floor window/door sections and an upper story with a dark window, light-colored ground floor of a central building with a large dark shop window displaying a red stylized 'I', a dark piano on the sidewalk, two dark doors to the right of the shop window, a small white flag hanging above, a dark upper story with two windows, a grey stone column with a circular red and white sign attached, a dark reddish-brown ground floor building with two dark doors, a dark upper story with a window, and a dark paved street.



Row of three traditional urban buildings with gabled roofs under a clear sky; leftmost building with reddish-brown brick facade, multiple rectangular dark-paned windows, one second-story window partially boarded with wood, and dark reddish-brown ground floor window frames; middle building with dark gray facade, white window frames and horizontal decorative trim, multiple large dark-paned rectangular windows, ground floor signage reading "KAARVERHUUR KANTOOR O.Z.A.B.", "WAL 52", and "020 5385421", large ground floor shop windows displaying bright red interiors, a central recessed entrance with numbers "67A" and "67B", and a small light fixture; rightmost building partially visible with dark gray facade, white trim, upper dark-paned windows, a ground floor shop window with bright red interior, and a white arrow sign pointing left.

(b) La-MixVPR

Figure 14. Qualitative comparison between MixVPR (top) and La-MixVPR (bottom) on the Amstertime dataset. La-MixVPR uses BGE-Large as the text encoder with CAT fusion. From left to right: Query, Top-1, Top-2, and Top-3 retrieved images. Green borders indicate a correct match, while red borders indicate an incorrect match.



(a) MixVPR



Large multi-story stone building with "DE BIJENKORF" sign, ornate street lamp, multi-story brick building with "CHANGE" sign, multi-story brick building with "Marlboro" sign.

Large multi-story commercial building with light stone and red brick facade, prominent "DE BIJENKORF" sign, large ground-level display windows and arched entrances, paved sidewalk, wide street with multiple tram tracks embedded in patterned paving, overhead tram wires, row of multi-story traditional European buildings with varied facades and ground-level storefronts, paved sidewalk, distant ornate buildings.

Multi-story brick building with white-framed windows and ornate white molding on the left, a red and white "1HOUR SERVICE" sign visible on the lower left, a narrow urban street foreground, a multi-story light-colored building with large white-framed windows on the right, a green oval 'Grolsch' sign and a red oval 'Haverlaar cafe' sign hanging on the right building, an ornate stone archway with sculptures at the end of the street, a multi-pane glass roof building visible beyond the archway, a dark elongated object suspended by wires high overhead.

Ornate multi-story historic building with "BIJENKORF" visible on facade, tall grey pole with yellow flags and pedestrian sign, green deciduous trees, modern multi-story building with grey facade and vertical lettering "VERLIUM" visible, large white obelisk monument with sculptures at base, white stone lion sculpture on pedestal, multi-story brown building.

(b) La-MixVPR

Figure 15. Qualitative comparison between MixVPR (top) and La-MixVPR (bottom) on the Amstertime dataset. La-MixVPR uses BGE-Large as the text encoder with CAT fusion. From left to right: Query, Top-1, Top-2, and Top-3 retrieved images. Green borders indicate a correct match, while red borders indicate an incorrect match.

**Query:**  
 Ornate multi-story building with a rounded bay window on the left, intricate facade details, signs "LEVEN VERZEKERING MAATSCHAPPIJ UTRECHT" and "UTRECHT", ground floor shopfront with "doke" lettering, taller building with a distinct stepped gable roof and large windows, vertical sign "JEUPENS" on its facade, horizontal sign "LINDBEIGH" below it, row of multi-story buildings with varied gabled roofs extending to the right.

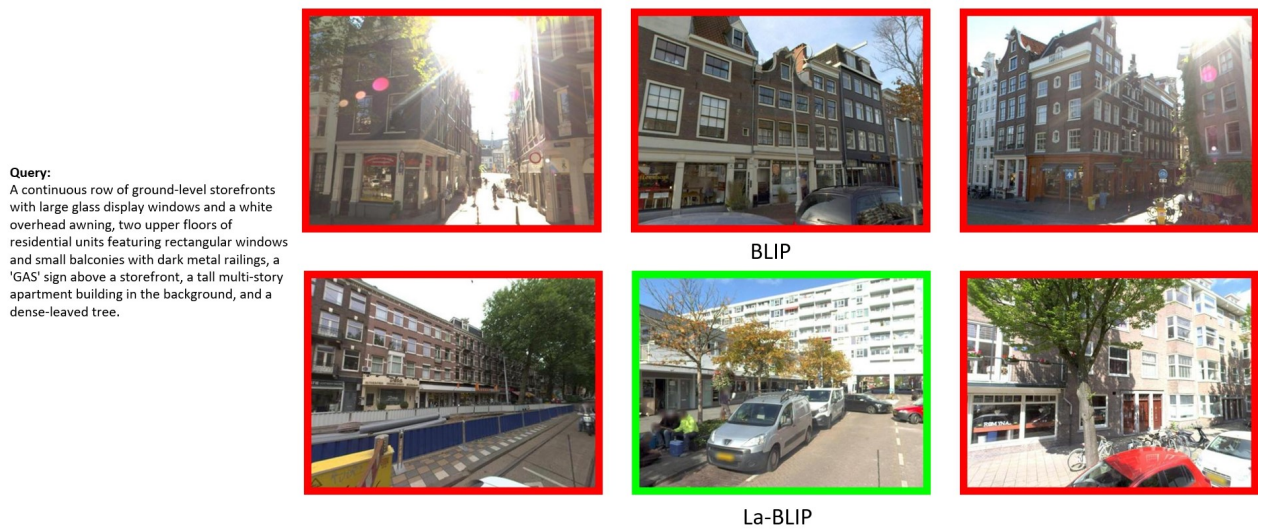


Figure 16. Cross-Modal retrieval (Amstertime dataset): we use a textual query (left) to retrieve geo-tagged images from a reference database. We present the top-3 results when using BLIP (top) and La-BLIP (bottom). Green borders indicate a correct match, while red borders indicate an incorrect match.

**Query:**  
 Paved foreground with square dark gray paving stones, light-colored brick building with a window, vertical section of darker bricks, dark wooden door with the number "170", sign above the door with Arabic script and "MOSQUEE EL OUMMA EL ISLAMIA", bare tree, building with a "CINEMA CINEMA" marquee sign listing movie titles.



Figure 17. Cross-Modal retrieval (Amstertime dataset): we use a textual query (left) to retrieve geo-tagged images from a reference database. We present the top-3 results when using BLIP (top) and La-BLIP (bottom). Green borders indicate a correct match, while red borders indicate an incorrect match.



*Figure 18.* Cross-Modal retrieval (Amstertime dataset): we use a textual query (left) to retrieve geo-tagged images from a reference database. We present the top-3 results when using BLIP (top) and La-BLIP (bottom). Green borders indicate a correct match, while red borders indicate an incorrect match.